iScience, Volume *26*

Supplemental information

A consortium of three-bacteria isolated from human feces inhibits formation of atherosclerotic deposits and lowers lipid levels in a mouse model

Zhuye Jie, Qian Zhu, Yuanqiang Zou, Qili Wu, Min Qin, Dongdong He, Xiaoqian Lin, Xin Tong, Jiahao Zhang, Zhu Jie, Wenwei Luo, Xiao Xiao, Shiyu Chen, Yonglin Wu, Gongjie Guo, Shufen Zheng, Yong Li, Weihua Lai, Huanming Yang, Jian Wang, Liang Xiao, Jiyan Chen, Tao Zhang, Karsten Kristiansen, Huijue Jia, and Shilong Zhong

Supplementary Materials

Figure S1. Western diet-fed *Apoe*$^{-/-}$ mice treated with live bacteria exhibited smaller LV volume and diameter at end-systole and diastole and better cardiac function; related to Figure 2 and Table S2.

Figure S2. Changes of differentially expressed genes in mice of different groups; related to Figure 3 and Table S4.

Figure S3. OPLS-DA loading plots for different groups; related to Figure 4.

Figure S4. Changes of plasma metabolites in mice of the different groups; related to Figure 4 and Table S9.

Figure S5. Causality analysis between the plasma metabolites and lipids; related to STAR Method and Table S10.

Figure S6. Boxplots of metabolites previously reported to play important role in cardiovascular disease, related to Figure 4 and Table S9.

Figure S7. Changes in the fecal microbiome; related to Figure 5 and Table S13.

Figure S8. DMM clustering of metagenomic data (n = 476); related to Figure 5 and Table S13.

Figure S9. Change in functional potential based on shotgun sequencing data; related to STAR Method and Table S14.

Figure S10. Change in the 7*α*-dehydroxylation pathway; related to Figure 6 and Table S14.

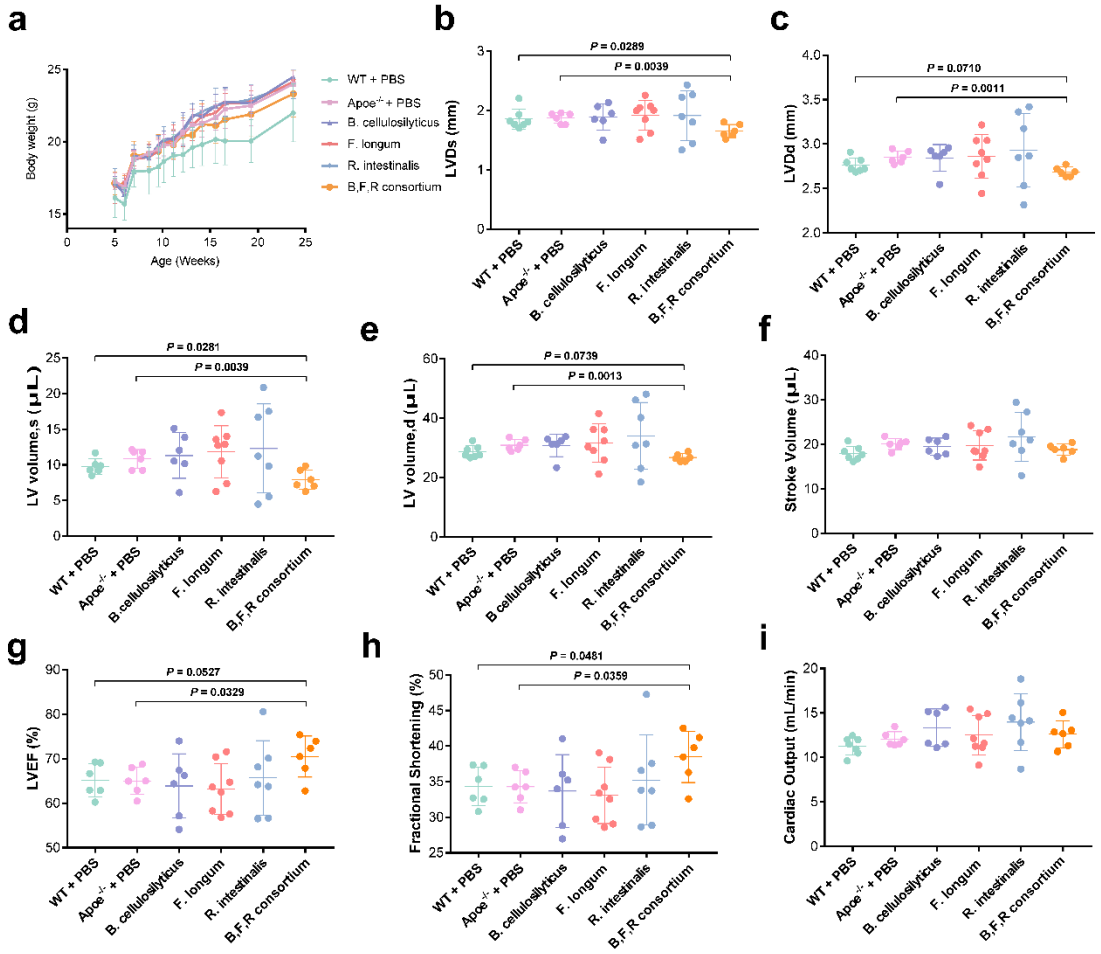

Figure S1. Western diet-fed Apoe$^{-/-}$ mice treated with live bacteria exhibited smaller LV volume and diameter at end-systole and diastole and better cardiac function; related to Figure 2 and Table S2. a, Body weight changes over the course of the experimental period (6 to 8 samples per group). **b-i**, Comparison of animal ultrasonography in heart (6 to 8 samples per group). LVDs, left ventricular end-systolic dimension; LVDd, left ventricular end- diastolic dimension; LV volume, s, left ventricular end-diastolic volume; LV volume, d, left ventricular end-systolic volume; LVEF, left ventricular ejection fraction. Two-tailed Student's t-test or Mann-Whitney U-test was used for comparison between two groups. Data are shown as mean ± standard error of the mean.

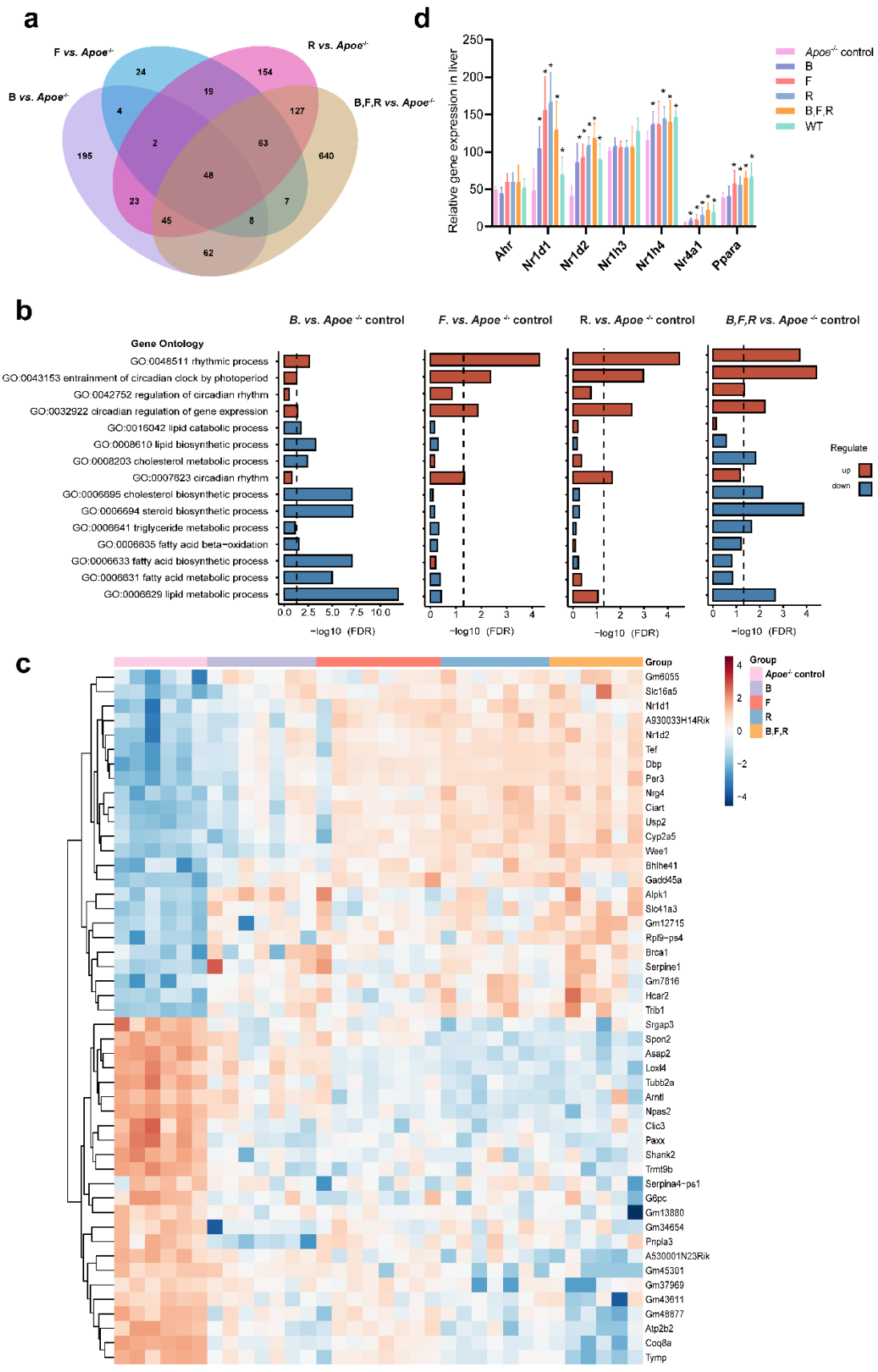
a
F vs. Apoe-/-
R vs. Apoe-/-
B vs. Apoe-/-
B,F,R vs. Apoe-/-
24
154
19
4
127
2
63
640
195
48
23
7
45
8
62
d
Relative gene expression in liver
250
200
150
100
50
0
Apoe-/- control
B
F
R
B,F,R
WT
Ahr
Nr1d1
Nr1d2
Nr1h3
Nr1h4
Nr4a1
Ppara
b
B. vs. Apoe -/- control
F. vs. Apoe -/- control
R. vs. Apoe -/- control
B,F,R vs. Apoe -/- control
Gene Ontology
GO:0048511 rhythmic process
GO:0043153 entrainment of circadian clock by photoperiod
GO:0042752 regulation of circadian rhythm
GO:0032922 circadian regulation of gene expression
GO:0016042 lipid catabolic process
GO:0008610 lipid biosynthetic process
GO:0008203 cholesterol metabolic process
GO:0007623 circadian rhythm
GO:0006695 cholesterol biosynthetic process
GO:0006694 steroid biosynthetic process
GO:0006641 triglyceride metabolic process
GO:0006635 fatty acid beta-oxidation
GO:0006633 fatty acid biosynthetic process
GO:0006631 fatty acid metabolic process
GO:0006629 lipid metabolic process
0.0 2.5 5.0 7.5 10.0
0 1 2 3 4
−log10 (FDR)
Regulate
up
down
c
Group
Apoe-/- control
B
F
R
B,F,R
4
2
0
−2
−4
Gm6055
Slc16a5
Nr1d1
A930033H14Rik
Nr1d2
Tef
Dbp
Per3
Nrg4
Ciart
Usp2
Cyp2a5
Wee1
Bhlhe41
Gadd45a
Alpk1
Slc41a3
Gm12715
Rpl9-ps4
Brca1
Serpine1
Gm7816
Hcar2
Trib1
Srgap3
Spon2
Asap2
Loxl4
Tubb2a
Arntl
Npas2
Clic3
Paxx
Shank2
Trmt9b
Serpina4-ps1
G6pc
Gm13880
Gm34654
Pnpla3
A530001N23Rik
Gm45301
Gm37969
Gm43611
Gm48877
Atp2b2
Coq8a
Tymp

Figure S2. Changes of differentially expressed genes in mice of different groups; related to Figure 3 and Table S4. a, Venn diagram of the differentially expressed genes of the liver transcriptome in each group. **b**, Results of GSEA of Gene Ontologies revealed the variation of lipogenic and circadian rhythm pathways. **c**, The heatmap of 48 overlapping genes in four groups treated with live bacteria. **d**, Changes of key nuclear receptor genes involved in lipogenic. The differentially expressed genes were defined as FDR value smaller than 0.05 and the absolute value of fold change larger than 1. WT, western diet-fed normal C57BL/6 mice treated with vehicle (n = 7); *Apoe*$^{-/-}$ control, western diet-fed *Apoe*$^{-/-}$ mice treated with vehicle (n = 6); B, western diet-fed *Apoe*$^{-/-}$ mice treated with *B. cellulosilyticus* (n = 7); F, western diet-fed *Apoe*$^{-/-}$ mice treated with *F. longum* (n = 8); R, western diet-fed *Apoe*$^{-/-}$ mice treated with *R. intestinalis* (n = 7); B,F,R, western diet–fed *Apoe*$^{-/-}$ mice treated with the consortium of the three bacteria (n = 5).

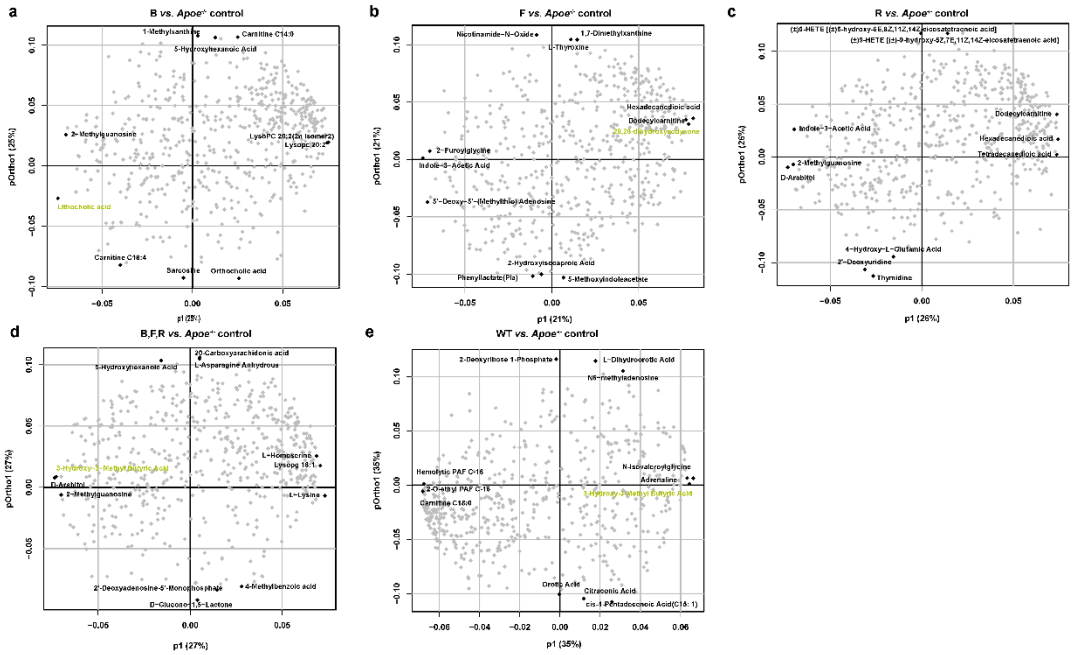

Figure S3. OPLS-DA loading plots for different groups; related to Figure 4. WT, western diet-fed normal C57BL/6J mice treated with vehicle (n = 7); *Apoe*$^{-/-}$ control, western diet-fed *Apoe*$^{-/-}$ mice treated with vehicle (n = 6); B, western diet-fed *Apoe*$^{-/-}$ mice treated with *B. cellulosilyticus* (n = 7); F, western diet-fed *Apoe*$^{-/-}$ mice treated with *F. longum* (n = 8); R, western diet-fed *Apoe*$^{-/-}$ mice treated with *R. intestinalis* (n = 7); B,F,R, western diet-fed *Apoe*$^{-/-}$ mice treated with the consortium of the three bacteria (n = 5).

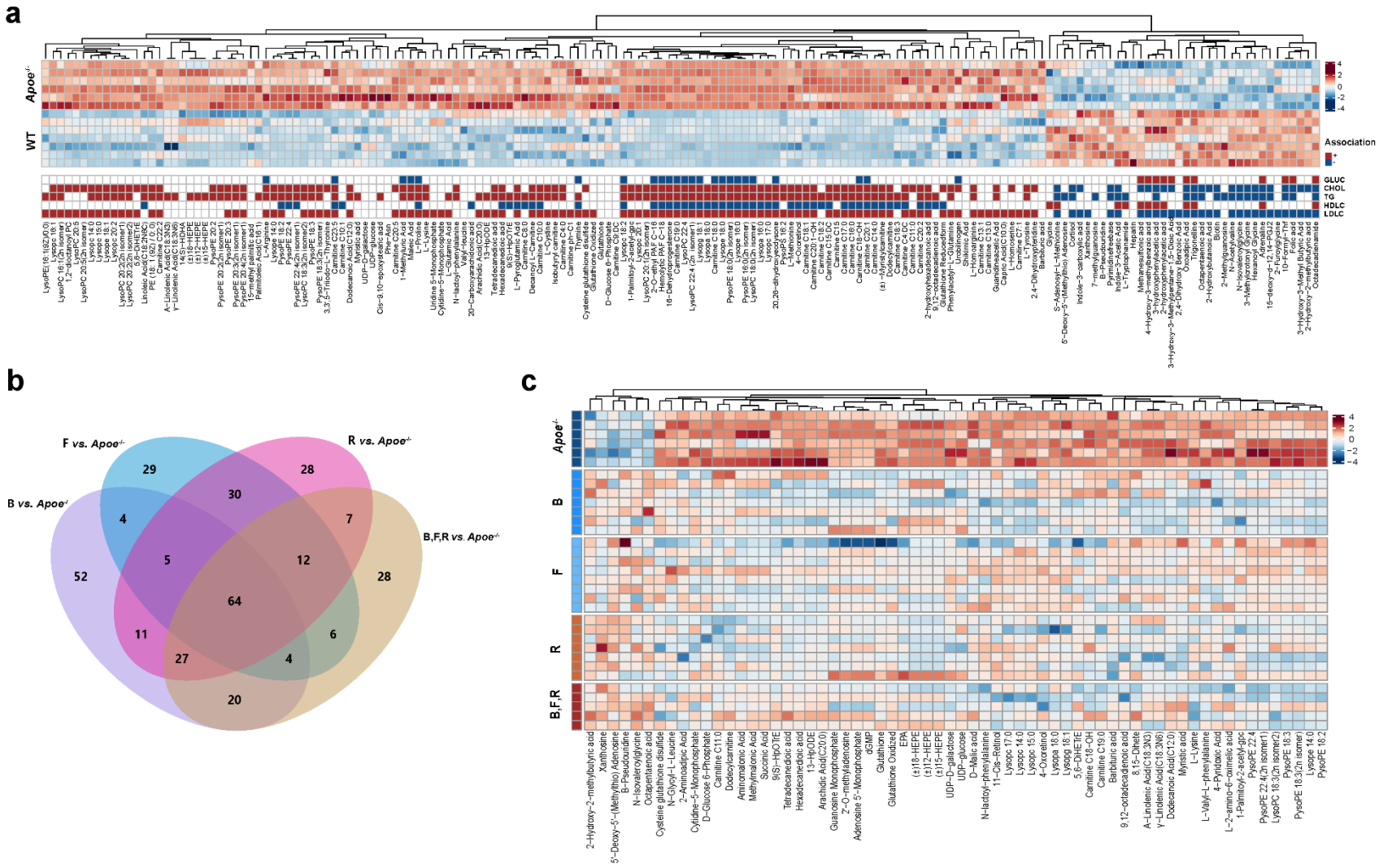
a
Apoe-/-
WT
Association
GLUC
CHOL
TG
HDLC
LDLC
b
F vs. Apoe-/-
R vs. Apoe-/-
B vs. Apoe-/-
B,F,R vs. Apoe-/-
29
28
30
4
7
5
12
52
28
64
11
6
27
4
20
c
Apoe-/-
B
F
R
B,F,R

Figure S4. Changes of plasma metabolites in mice of the different groups; related to Figure 4 and Table S9. a, The heatmap of metabolites differing in abundance between WT and *Apoe*$^{-/-}$ control groups. The grids filled with graduated color indicate the relative abundance of metabolites, and the grids filled with pure red and blue represent the correlation between metabolites and lipids. **b**, Venn diagrams of the intersecting metabolites differing in abundance in the groups treated with live bacteria. **c**, The heatmaps of the intersecting metabolites differing in abundance in the groups treated with live bacteria. The metabolites differing in abundance were defined as *P* value smaller than 0.05 and the VIP value larger than 1. Two-tailed Student's t-test was used for comparison between two groups. WT, western diet-fed normal C57BL/6J mice treated with vehicle (n = 7); *Apoe*$^{-/-}$ control, western diet-fed *Apoe*$^{-/-}$ mice treated with vehicle (n = 6); B, western diet-fed *Apoe*$^{-/-}$ mice treated with *B. cellulosilyticus* (n = 7); F, western diet-fed *Apoe*$^{-/-}$ mice treated with *F. longum* (n = 8); R, western diet-fed *Apoe*$^{-/-}$ mice treated with *R. intestinalis* (n = 7); B,F,R, western diet-fed *Apoe*$^{-/-}$ mice treated with the consortium of the three bacteria (n = 5). GLUC, glucose; TG, triglycerides; LDLC, low-density lipoprotein cholesterol; HDLC, high-density lipoprotein cholesterol; CHOL, total cholesterol.

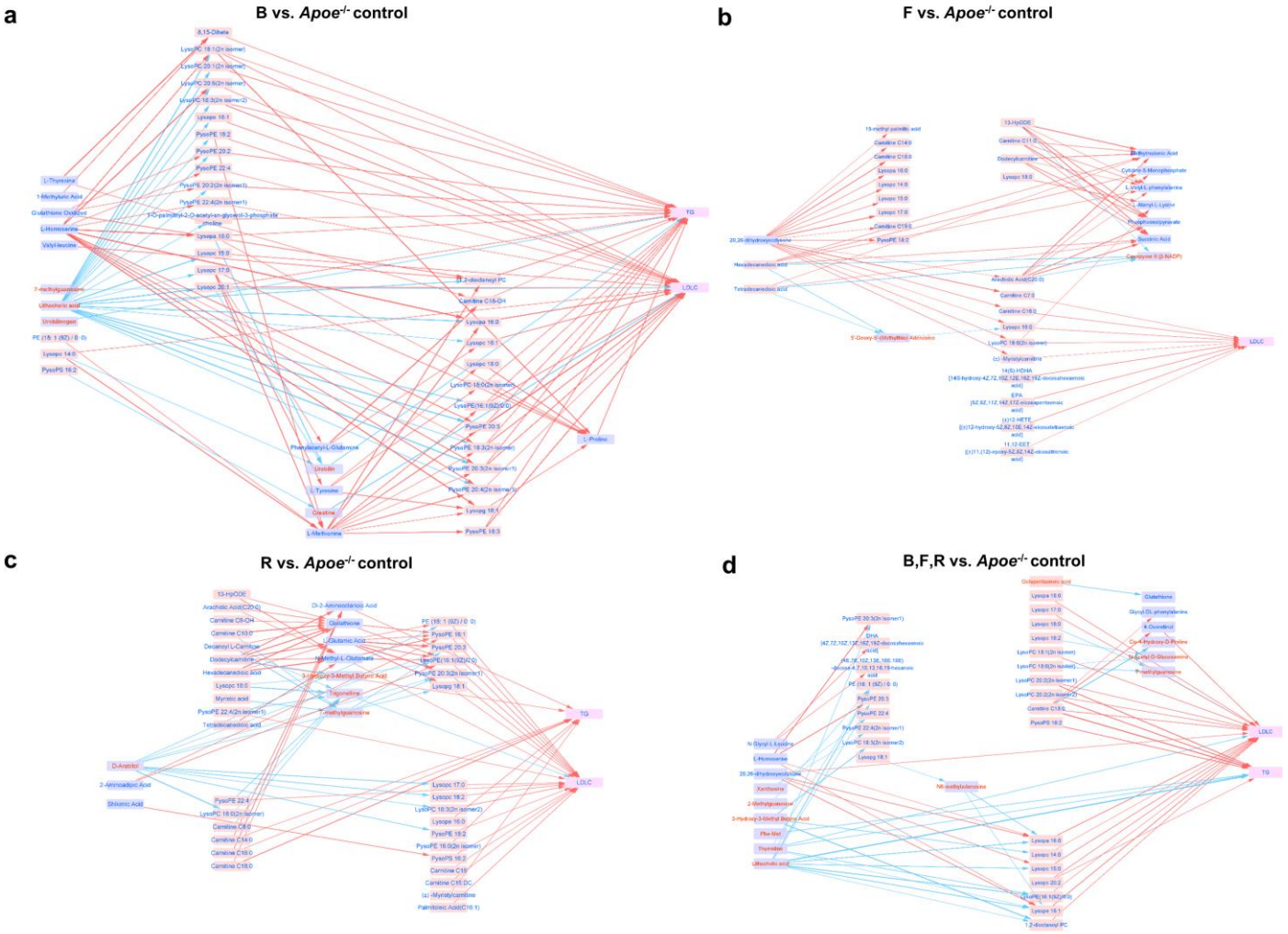
a
B vs. Apoe-/- control
8,15-DiHete
LysoPC 18:1(2n isomer)
LysoPC 20:1(2n isomer)
LysoPC 20:5(2n isomer)
LysoPC 18:3(2n isomer2)
Lysopc 16:1
PysoPE 18:2
PysoPE 20:2
PysoPE 22:4
PysoPE 20:2(2n isomer3)
PysoPE 22:4(2n isomer1)
1-O-palmitoyl-2-O-acetyl-sn-glycerol-3-phosph ate
choline
Lysopa 18:0
Lysopc 15:0
Lysopc 17:0
Lysopc 20:1
L-Thyroxine
1-Methyluric Acid
Glutathione Oxidized
L-Homocystine
Valyl-leucine
7-methylguanosine
Ursodeoxycholic acid
Urobilinogen
PE (15: 1 (5Z) / 0: 0)
Lysopc 14:0
PysoPS 18:2
TG
LDLC
L-Proline
Phenylacetyl-L-Glutamine
Urobilin
L-Tyrosine
Creatine
L-Methionine
18:2-dioctanoyl PC
Carnitine C18-OH
Lysopa 18:0
Lysopc 18:1
Lysopc 18:0
LysoPC 18:0(2n isomer)
LysoPE(16:1(9Z)/0:0)
PysoPE 20:3
PysoPE 18:3(2n isomer)
LysoPE 20:3(2n isomer1)
PysoPE 20:4(2n isomer1)
Lysopg 18:1
PysoPE 18:3
b
F vs. Apoe-/- control
15-methyl palmitic acid
Carnitine C14:0
Carnitine C18:0
Lysopa 16:0
Lysopc 14:0
Lysopc 15:0
Lysopc 17:0
Carnitine C19:0
PysoPE 18:2
20,26-dihydroxycholesterol
Hexadecanedioic acid
Tetradecanedioic acid
5'-Deoxy-5'-(Methylthio) Adenosine
13-HpODE
Carnitine C11:0
Dodecylcarnitine
Lysopc 18:0
Arachidic Acid(C20:0)
Carnitine C7:0
Carnitine C16:0
Lysopc 16:0
LysoPC 18:0(2n isomer)
(2)-Myristylcarnitine
14(S)-HDHA
[14S-hydroxy-4Z,7Z,10Z,12E,16Z,19Z-docosahexaenoic acid]
EPA
[5Z,8Z,11Z,14Z,17Z-eicosapentaenoic acid]
(±)12-HETE
[(±)12-hydroxy-5Z,8Z,10E,14Z-eicosatetraenoic acid]
11,12-EET
[(±)11,(12)-epoxy-5Z,8Z,14Z-eicosatrienoic acid]
Ethylmalonic Acid
Cytosine-5-Monophosphate
Lysyl-L-phenylalanine
Alanyl-L-Lysine
Phosphoenolpyruvate
Succinic Acid
Cytochrome B (3 NADP)
LDLC
c
R vs. Apoe-/- control
13-HpODE
Arachidic Acid(C20:0)
Carnitine C8-OH
Carnitine C10:0
Decanoyl L-Carnitine
Dodecylcarnitine
Hexadecanedioic acid
Lysopc 18:0
Myristic acid
PysoPE 22:4(2n isomer1)
Tetradecanedioic acid
D-Arabitol
2-Aminoadipic Acid
Shikimic Acid
Di-2-Aminooctanoic Acid
Glutathione
L-Glutamic Acid
N-Methyl-L-Glutamate
3-Hydroxy-3-Methyl Butyric Acid
Threonine
7-methylguanosine
PysoPE 22:4
LysoPC 18:0(2n isomer)
Carnitine C8:0
Carnitine C14:0
Carnitine C16:0
Carnitine C18:0
PC (16: 1 (9Z) / 0: 0)
PysoPE 16:1
PysoPE 20:3
LysoPE(16:1(9Z)/0:0)
LysoPE 20:3(2n isomer1)
Lysopg 18:1
Lysopc 17:0
Lysopc 18:2
LysoPC 18:3(2n isomer2)
Lysopa 18:0
PysoPE 18:2
PysoPE 16:0(2n isomer)
PysoPS 16:2
Carnitine C15
Carnitine C15 DC
(±) -Myristylcarnitine
Palmitoleic Acid(C16:1)
TG
LDLC
d
B,F,R vs. Apoe-/- control
PysoPE 20:3(2n isomer1)
DHA
[4Z,7Z,10Z,13Z,16Z,19Z-docosahexaenoic acid]
PE (16: 1 (9Z) / 0: 0)
PysoPE 20:3
PysoPE 22:4
PysoPE 22:4(2n isomer1)
LysoPC 18:3(2n isomer2)
Lysopg 18:1
N-Oxyal-L-Lysine
L-Homocystine
20,26-dihydroxycholesterol
Xanthosine
2-Methylguanosine
3-Hydroxy-3-Methyl Butyric Acid
Phe-Met
Thymidine
Ethosuximide
Octapentaenoic acid
Lysopa 18:0
Lysopc 17:0
Lysopc 18:0
Lysopc 18:2
LysoPC 18:1(2n isomer)
LysoPC 18:0(2n isomer)
LysoPC 20:2(2n isomer1)
LysoPC 20:2(2n isomer2)
Carnitine C18:0
PysoPS 18:2
Glutathione
Glycyl-DL-phenylalanine
4-Oxosphinol
Cis-4-Hydroxy-D-Proline
N-Acetyl-D-Glucosamine
7-methylguanosine
N6-methyladenosine
Lysopa 18:0
Lysopc 14:0
Lysopc 15:0
Lysopc 20:2
PysoPE 16:1(9Z)/0:0)
Lysopg 18:1
1,2-dioctanoyl PC
LDLC
TG

Figure S5. Causality analysis between the plasma metabolites and lipids; related to STAR Method and Table S10. The arrow "A→B" indicates that A had a potential regulatory effect on B, and the thickness of the line indicates the level of potential causality. The color of the line reflects the correlation between the two nodes, of which red is a positive correlation and blue is a negative correlation. The color of the text indicates the change in the level of metabolites and lipids, with red representing upregulation and blue representing downregulation. *Apoe*$^{-/-}$ control, western diet-fed *Apoe*$^{-/-}$ mice treated with vehicle (n = 6); B, western diet-fed *Apoe*$^{-/-}$ mice treated with *B. cellulosilyticus* (n = 7); F, western diet-fed *Apoe*$^{-/-}$ mice treated with *F. longum* (n = 8); R, western diet-fed *Apoe*$^{-/-}$ mice treated with *R. intestinalis* (n = 7); B,F,R, western diet-fed *Apoe*$^{-/-}$ mice treated with the consortium of the three bacteria (n = 5). TG, triglycerides; LDLC, low-density lipoprotein cholesterol.

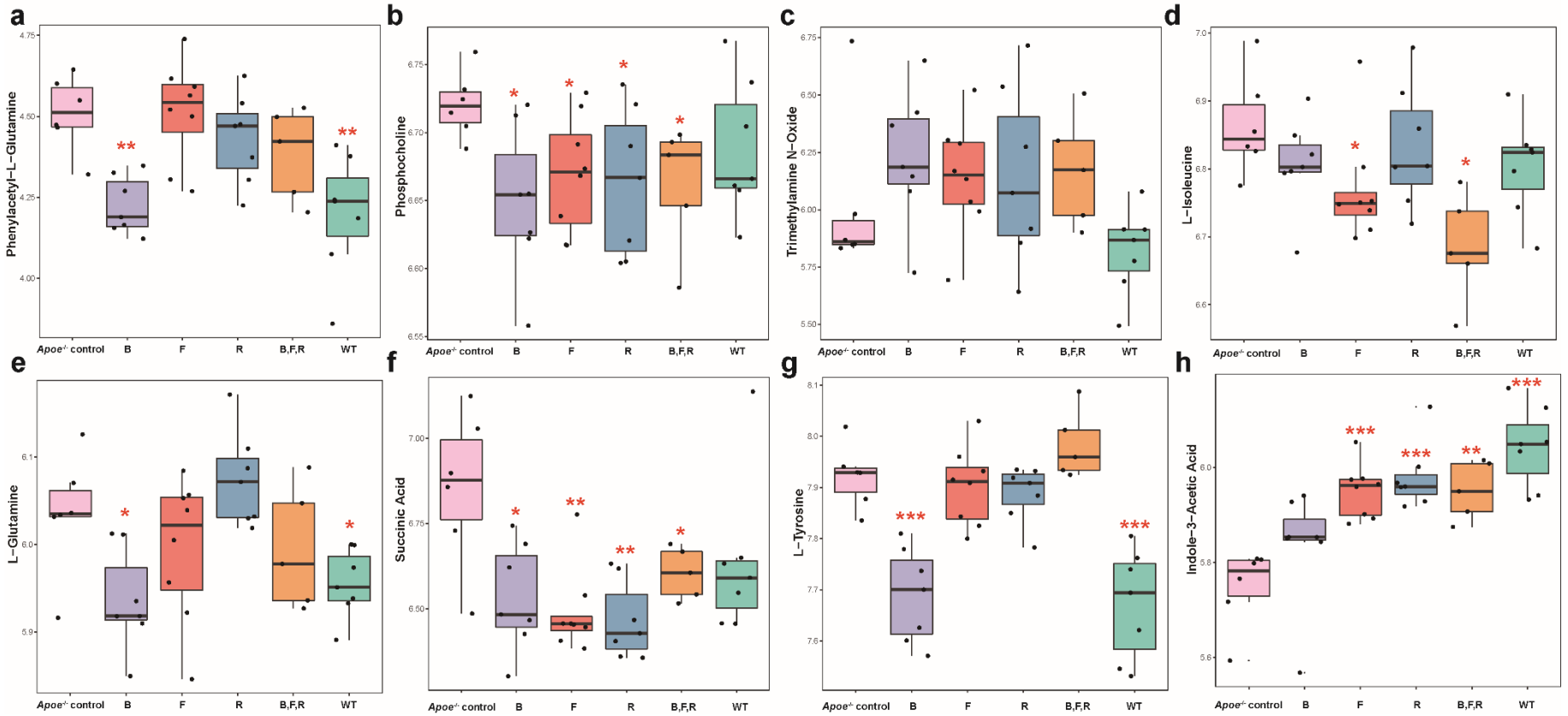

Figure S6. Boxplots of metabolites previously reported to play important role in cardiovascular disease, related to Figure 4 and Table S9. a, Phenylacetyl−L−Glutamine. **b**, Phosphocholine. **c**, Trimethylamine N−Oxide. **d**, L−Isoleucine. **e**, L−Glutamine. **f**, Succinic Acid. **g**, L−Tyrosine and. **h**, Indole−3−Acetic Acid in mice of different groups. WT, western diet-fed normal C57BL/6J mice treated with vehicle (n = 7); *Apoe*$^{-/-}$ control, western diet-fed *Apoe*$^{-/-}$ mice treated with vehicle (n = 6); B, western diet-fed *Apoe*$^{-/-}$ mice treated with *B. cellulosilyticus* (n = 7); F, western diet-fed *Apoe*$^{-/-}$ mice treated with *F. longum* (n = 8); R, western diet-fed *Apoe*$^{-/-}$ mice treated with *R. intestinalis* (n = 7); B,F,R, western diet-fed *Apoe*$^{-/-}$ mice treated with the cocktail of the three bacteria (n = 5). *P<0.05, ** P<0.01, *** P<0.001 vs *Apoe*$^{-/-}$ control in t-test.

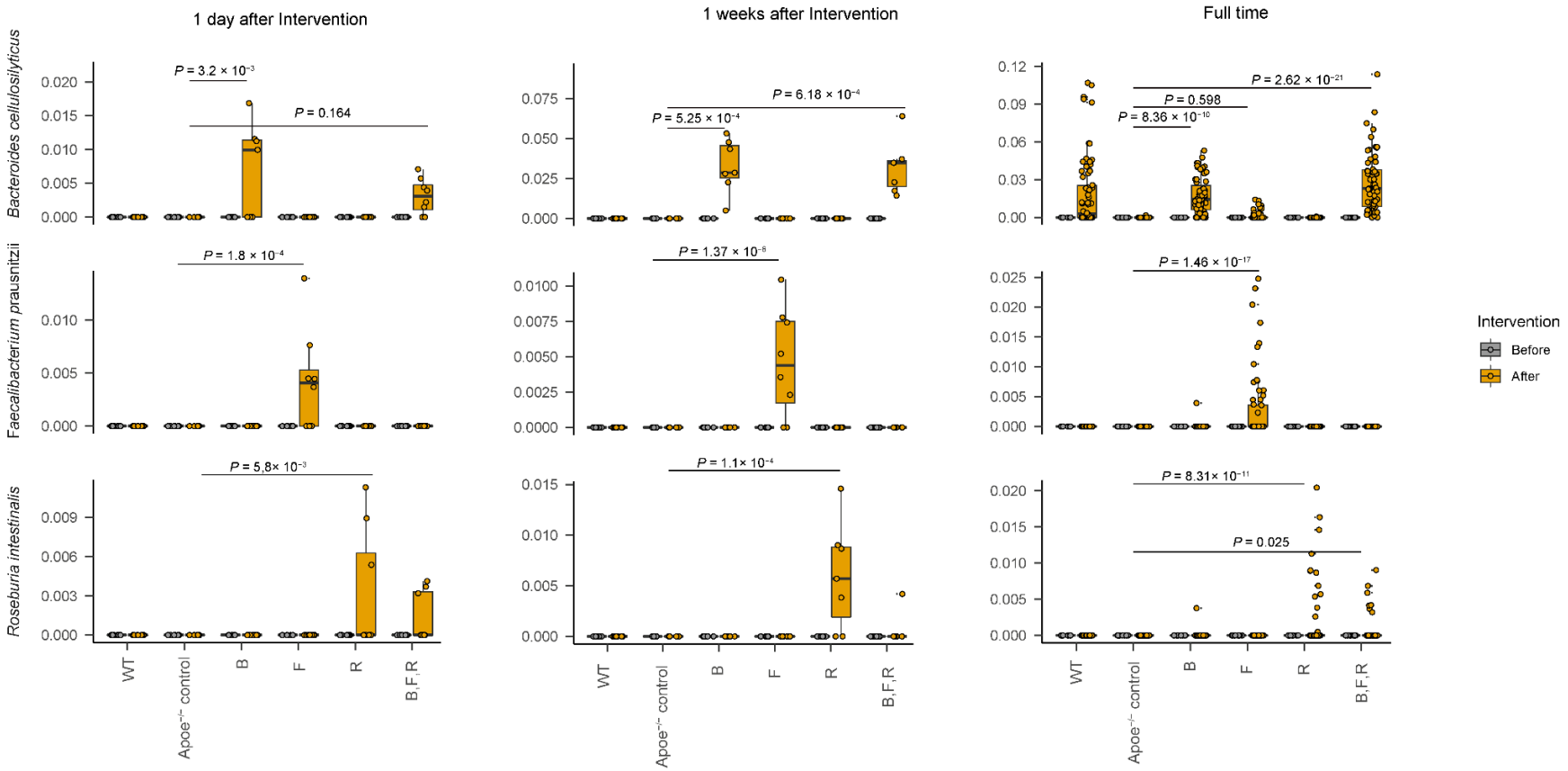

Figure S7. Changes in the fecal microbiome; related to Figure 5 and Table S13. *B. cellulosilyticus*, *R. intestinalis* and *F. longum* abundances in feces evaluated by metagenomic sequencing. The box depicts the interquartile range (IQR) between the first and third quartiles (25th and 75th percentiles, respectively), and the line inside denotes the median, whereas the points represent the relative abundance (asin sqrt transform) in each sample. For 1 day

after intervention and 1 weeks after intervention, the p-value indicates the ANOVA test between groups. For Full time, the p-value indicates the linear mix model test between groups, ref group is control (*Apoe*$^{-/-}$ control), random effect is the subject of mouse. We could not detect the three bacteria in the 4 groups at baseline and *Apoe*$^{-/-}$ control group along the time flow of experiment, whereas supplementation with a single species or the consortium significantly increased the relative abundance of the three bacteria recovered in the feces of *Apoe*$^{-/-}$ mice.

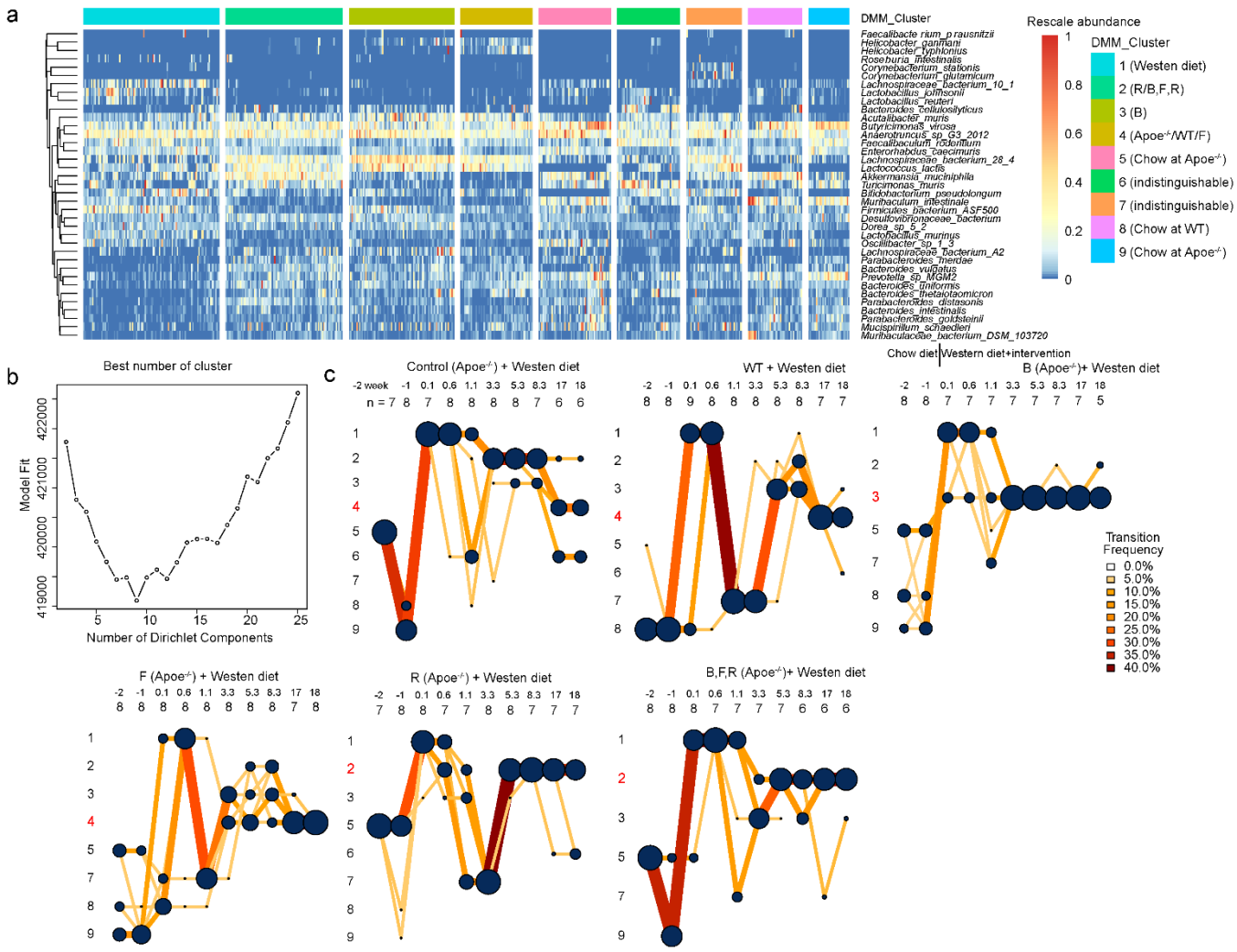
a
DMM_Cluster
Faecalibacte rium_p rausnitzii
Helicobacter_ganmani
Helicobacter_typhlonius
Roseburia_intestinalis
Corynebacterium_stationis
Corynebacterium_glutamicum
Lachnospiraceae_bacterium_10_1
Lactobacillus_johnsonii
Lactobacillus_reuteri
Bacteroides_cellulosilyticus
Acutalibacter_muris
Butyricimonas_virosa
Anaerotruncus_sp_G3_2012
Faecalibaculum_rodentium
Enterorhabdus_caecimuris
Lachnospiraceae_bacterium_28_4
Lactococcus_lactis
Akkermansia_muciniphila
Turicimonas_muris
Bifidobacterium_pseudolongum
Muribaculum_intestinale
Firmicutes_bacterium_ASF500
Desulfovibrionaceae_bacterium
Dorea_sp_5_2
Lactobacillus_murinus
Oscillibacter_sp_1_3
Lachnospiraceae_bacterium_A2
Parabacteroides_merdae
Bacteroides_vulgatus
Prevotella_sp_MGM2
Bacteroides_uniformis
Bacteroides_thetaiotaomicron
Parabacteroides_distasonis
Bacteroides_intestinalis
Parabacteroides_goldsteinii
Mucispirillum_schaedleri
Muribaculaceae_bacterium_DSM_103720
Rescale abundance
1
0.8
0.6
0.4
0.2
0
DMM_Cluster
1 (Westen diet)
2 (R/B,F,R)
3 (B)
4 (Apoe-/-/WT/F)
5 (Chow at Apoe-/-)
6 (indistinguishable)
7 (indistinguishable)
8 (Chow at WT)
9 (Chow at Apoe-/-)
Chow diet
Western diet+intervention
b
Best number of cluster
Model Fit
422000
421000
420000
419000
5
10
15
20
25
Number of Dirichlet Components
c
Control (Apoe-/-) + Westen diet
WT + Westen diet
B (Apoe-/-)+ Westen diet
F (Apoe-/-) + Westen diet
R (Apoe-/-) + Westen diet
B,F,R (Apoe-/-)+ Westen diet
-2 week -1 0.1 0.6 1.1 3.3 5.3 8.3 17 18
n = 7 8 7 8 8 8 8 7 6 6
Transition Frequency
0.0%
5.0%
10.0%
15.0%
20.0%
25.0%
30.0%
35.0%
40.0%

Figure S8. DMM clustering of metagenomic data (n = 476) ; related to Figure 5 and Table S13. A general overview of bacterial taxonomy development at each time point. **a**, Heatmap showing the relative abundance of the 35 most dominant bacterial species and our 3 supplemented bacteria. Top right panel shows the most dominant group per DMM cluster according to **c**. **b**, The appropriate number of clusters was determined based on the lowest Laplace approximation score. **c**, Transition model showing the progression of samples through each DMM cluster per each time point per group. Nodes are colored according to DMM cluster number and edges are colored by the transition frequency. Transitions with less than 4% frequency are not shown. The microbiota corresponding to mice receiving either a single bacterium or the consortium developed quickly into a stable phase distinct from that of the *Apoe*$^{-/-}$ control group, which fluctuated overtime. For example, at the stable phase, the *R. intestinalis* and the consortium group converged in the same cluster 2, while the *Apoe*$^{-/-}$ control group occupied cluster 4. These results indicated that supplementation with either a single species or the consortium affected the overall structure of the gut microbiota.

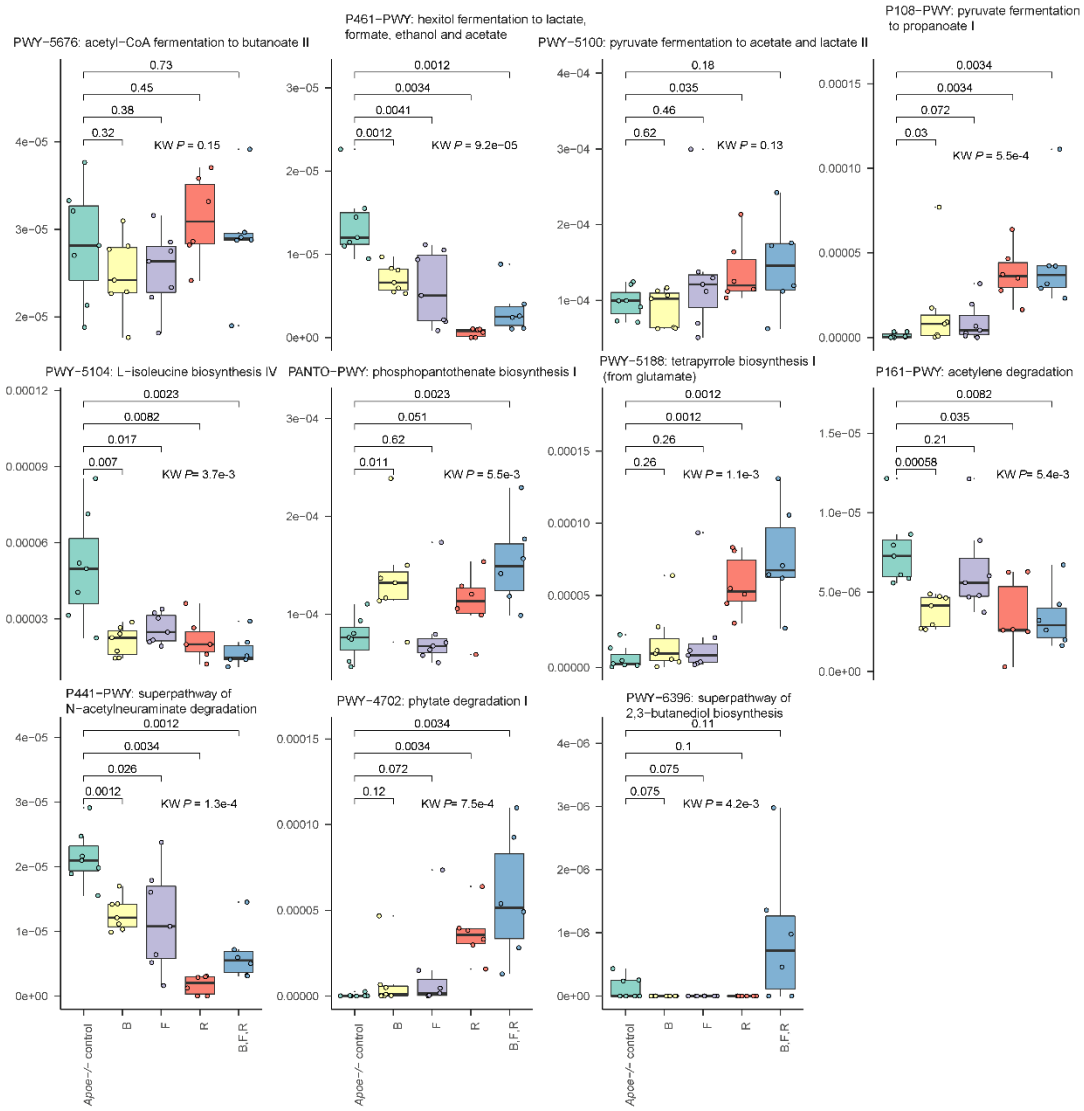

Figure S9. Change in functional potential based on shotgun sequencing data; related to STAR Method and Table S14. Pathways related to BCAA and SCFA. Phosphopantothenate biosynthesis I: valine, alanine -> coenzyme A. Tetrapyrrole biosynthesis I (from glutamate): glutamate -> vitamin B12. Acetylene degradation: acetylene-> ethanol, acetate. Super-pathway of N-acetylneuraminate degradation: N-acetylneuraminate -> formate, ethanol and acetate. Phytate degradation I: inositol -> butyrate. The box depicts the interquartile range (IQR) between the first and third quartiles (25th and 75th percentiles, respectively), and the line inside denotes the median, whereas the points represent the relative abundance in each sample. The p-values represent results of the Kruskal test and Wilcox test between groups.

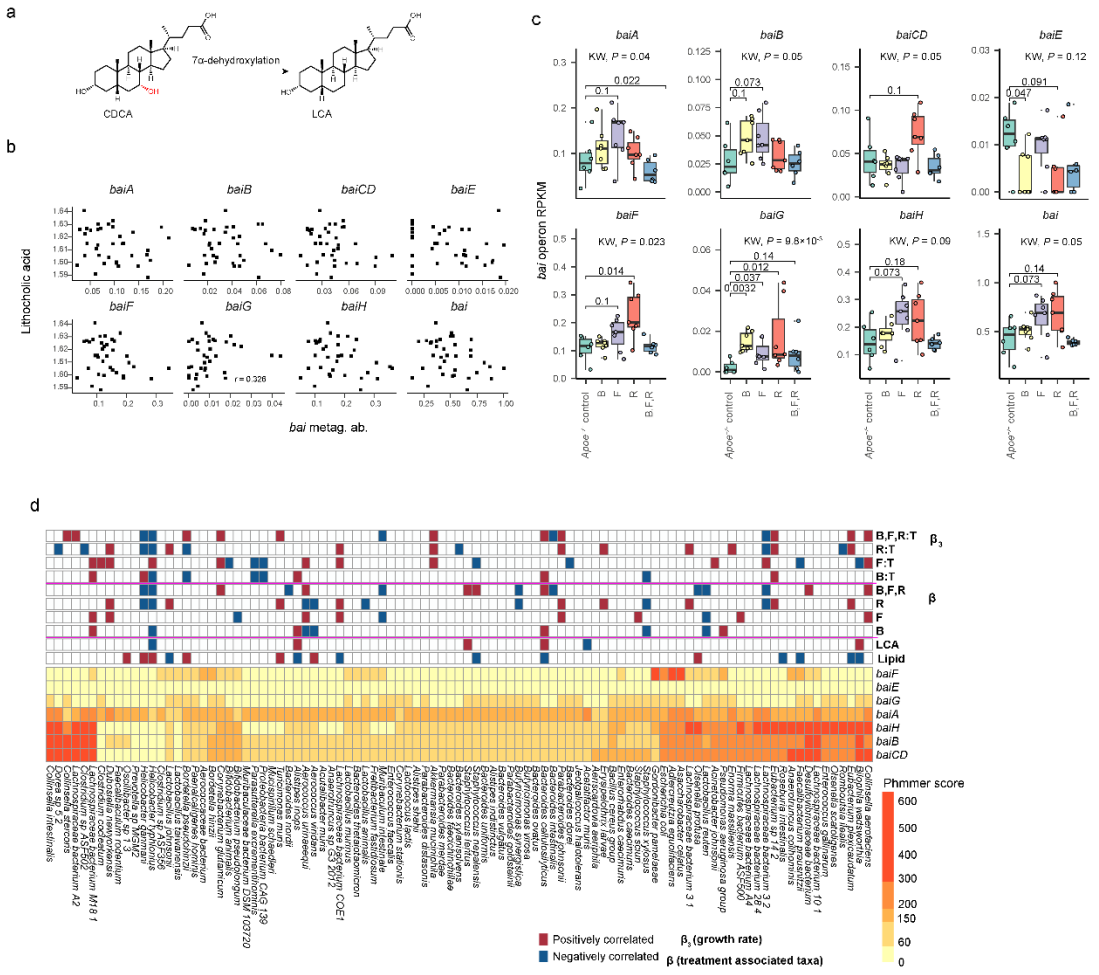

Figure S10. Change in the 7α-dehydroxylation pathway; related to Figure 6 and Table S14. a, *Bai* operon, which is known to contribute to the conversion from primary to secondary bile acids via the 7α-dehydroxylation pathway. **b**, *bai* metagenomic abundance was correlated with fecal LCA level by MS. **c**, *bai* metagenomic abundance was increased in the treatment groups, compared to the control group. **d**, Heatmap plot shows the bai gene cluster in taxa, each cell colored by phmmer score. Linear model was used for association between taxa and lipid parameter and metabolites. Relationship between taxon and treatment group was determined using the same model used in Figure 5c. Only q value<0.05 is shown.